Assessment of Human Biodistribution and Dosimetry of 4-Fluoro-11β-Methoxy-16α-^{18}F-Fluoroestradiol Using Serial Whole-Body PET/CT

Jean-Mathieu Beauregard, Étienne Croteau, Naseem Ahmed, Johan E. van Lier, and François Bénard

Sherbrooke Molecular Imaging Center (CIMS), Université de Sherbrooke, Sherbrooke, Quebec, Canada

4-Fluoro-11β-methoxy-16α-^{18}F-fluoroestradiol (4FMFES) is a newly developed radiolabeled estradiol analog for PET imaging of estrogen receptors (ERs) that shows improved target-to-background ratios, compared with 16α-^{18}F-fluoroestradiol (FES), in small-animal models. The aim of this study was to assess the biodistribution, dosimetry, and safety of 4FMFES in healthy women. **Methods:** Ten healthy subjects (6 pre- and 4 postmenopausal women) who had fasted were injected with 66–201 MBq of 4FMFES at a high effective specific activity (median, 251 GBq/μmol). During a 2-h period, each subject underwent 4 serial rapid PET acquisitions and 2 low-dose CT acquisitions on a PET/CT camera. Volumes of interest were drawn over source organs for each PET acquisition, allowing the calculation of time–activity curves, residence times, and radiation dosimetry estimates. Serial blood samples were obtained to measure blood and plasma activity clearance. 4FMFES safety was assessed by blood and urine analyses and vital-sign monitoring. **Results:** A 4FMFES injection was well tolerated in all subjects. The liver showed high uptake, and the hepatobiliary excretion was massive. Little urinary excretion occurred. Uterus uptake was visualized in all subjects and remained relatively constant over time (maximum and mean standardized uptake values at 60 min were 5.34 ± 3.32 and 2.68 ± 1.89, respectively). Background activity was low and decreased over time, resulting in an increasing uterus-to-background ratio (12.1 ± 2.2 at 60 min). The critical organ was the gallbladder (0.80 ± 0.51 mGy/MBq), followed by the upper large intestine (0.13 ± 0.04 mGy/MBq), small intestine (0.12 ± 0.04 mGy/MBq), and liver (0095 ± 0.019 mGy/MBq). For a typical 4FMFES dose of 185 MBq, the effective dose was calculated at 4.82 ± 0.70 mSv. **Conclusion:** 4FMFES is considered safe for use in humans, and its effective dose remains well within acceptable limits. The absorbed dose to the gallbladder was relatively high and could potentially be reduced by injecting 4FMFES in patients who had not fasted. 4FMFES showed a significant, potentially estrogen receptor–mediated uterus uptake in both pre- and postmenopausal subjects.

Received Aug. 14, 2008; revision accepted Oct. 8, 2008.
For correspondence or reprints contact: François Bénard, British Columbia Cancer Agency, Research Center Department of Molecular Oncology, Room 4.113, 675 West 10th Ave., Vancouver, BC, V5Z 1L3, Canada.
E-mail: fbenard@bccrc.ca
COPYRIGHT © 2009 by the Society of Nuclear Medicine, Inc.

Key Words: 4-fluoro-11β-methoxy-16α-^{18}F-fluoroestradiol; 16α-^{18}F-fluoroestradiol; estrogen receptor; breast cancer; positron emission tomography; radiation dosimetry

J Nucl Med 2009; 50:100–107
DOI: 10.2967/jnumed.108.057000

Scintigraphic imaging of estrogen receptors (ERs) is useful for in vivo tumor characterization in patients with breast cancer (*1*). To date, 16α-^{18}F-fluoroestradiol (FES) has been the most successful ER imaging agent for PET (*2*). 4-Fluoro-11β-methoxy-16α-^{18}F-fluoroestradiol (4FMFES) is a newly developed radiolabeled estradiol analog for ER imaging with PET (*3*). This tracer shows favorable biodistribution in small-animal experiments and achieves higher target–to–nontarget uptake ratios than does FES (*4,5*) and therefore appears promising for ER imaging in humans. The aim of this study was to assess the human biodistribution, establish the radiation dose estimates, and monitor the safety of 4FMFES. We also compared our dosimetry results with previously published data for FES (*6*). Preliminary results of this work have been presented elsewhere (*7*).

MATERIALS AND METHODS

Subjects

Ten healthy women (6 were premenopausal [age, 23–50 y], and 4 were postmenopausal [age, 52–64 y]) were recruited, and all gave informed consent to participate in this study. None of the postmenopausal subjects was undergoing hormone replacement therapy. Premenopausal subjects were imaged at the start of their menses, when the endogenous estrogens levels are at their lowest, or after 2–4 d of oral contraceptive withdrawal. Subjects fasted for at least 4 h before the 4FMFES injection. Two subjects (1 premenopausal and 1 postmenopausal) had undergone a cholecystectomy in the past. The study protocol was approved by Health Canada and the Human Research Ethics Committee of the Centre Hospitalier Universitaire de Sherbrooke.

Radiopharmaceutical

The precursor for 4FMFES was synthesized as previously described (*3*). ^{18}F-radiolabeling was performed using an optimized automated synthesis procedure (*8*). After purification by high-performance liquid

chromatography, the water–ethanol solution containing 4FMFES was sterilized by filtration (Millipore GS; 22-μm filter) and then diluted with normal saline to obtain a final ethanol concentration of 10% (<1 mL of ethanol per dose). The effective specific activity (ESA) at the end of synthesis (EOS) was measured as previously described (*9*). With the exception of 1 production batch in which the ESA at EOS was 28 GBq/μmol, the ESA of the 9 other batches ranged from 90 to 390 GBq/μmol, with a median ESA at EOS of 251 GBq/μmol. As recently reported, the implementation of our automated 4FMFES radiolabeling procedure resulted in high ESA values (*8,9*). A median dose of 174 MBq (range, 66–201 MBq) of 4FMFES was slowly injected over 2 min, and the intravenous line was thereafter flushed with normal saline. Median injected estradiol-equivalent mass, calculated from the decay-corrected ESA at the time of injection, was 1,141 pmol (range, 657–10,092 pmol).

Imaging

All images were acquired on a PET/CT camera (Gemini GXL 16; Philips). All acquisitions were performed from vertex to mid thighs, including the upper limbs. The first low-dose CT acquisition was started 5–10 min after the injection (120 kVp, 16 mAs), immediately followed by the first rapid PET acquisition (7–9 overlapping bed positions, 18 cm/bed position, 9-cm overlap, 1-min/bed position). Second and third PET acquisitions were performed at 30 and 60 min after injection, respectively. The subject was asked to stay still from the beginning of the first CT acquisition until the end of the third PET acquisition. The subject was then allowed to stand up, void, and rest and was rescanned at 120 min after injection with a second low-dose CT followed by a fourth PET acquisition. All PET images were reconstructed using a 3-dimensional line-of-response row-action maximum-likelihood algorithm with attenuation correction. The accuracy of the absolute count calibration of the scanner was validated against a uniform phantom containing ^{18}F-FDG at a known concentration. The measured activity was expressed as standardized uptake value (SUV = measured tissue activity concentration/[injected activity/patient weight]) for each voxel (64 μL).

Data Analysis

Using MIMvista software (version 4.0; MIMvista Corp.), we drew volumes of interest (VOIs) for each PET acquisition over the following source organs: liver, gallbladder, intestines (including small and large intestines), urinary bladder, and uterus. VOIs encompassing the whole-organ activity were obtained by using a lower SUV threshold on the PET images and then making fine adjustments with the aid of the fused anatomic images from the corresponding low-dose CT scan. For each source organ on the PET acquisition, the total normalized activity was expressed in decay-corrected percentage of injected dose (%ID). The residual injected activity not accounted for by any source organ was assumed to be distributed evenly in the remainder of the body (remainder of body %ID = 100% − $\%ID_{liver}$ − $\%ID_{gallbladder}$ − $\%ID_{intestine}$ − $\%ID_{uterus}$ − $\%ID_{urinary\ bladder}$). The %IDs of the source organs and of the remainder of body, as a function of time after injection, were entered in OLINDA software (Vanderbilt University), which is a complete software for internal dosimetry assessment that integrates updated physical models and dose factors (*10*). Biologic time–activity curves were then generated by curve fitting (1–3 exponential terms). The integration of the areas under the time–activity curves multiplied by the ^{18}F physical decay curve gave the residence times (calculated number of disintegrations occurring in the organ per becquerel injected). The voiding urinary bladder model (voiding interval, 3 h) and International Commission on Radiological Protection 30 gastrointestinal model (activity entering small intestine) were subsequently applied to account for urinary voiding and intestinal transit. Dosimetry estimates for the adult female model (56.9 kg) were then calculated for each individual subject with OLINDA software and averaged among subjects thereafter. The effective dose (ED), that is, the sum of the appropriately weighted organs, was also calculated with OLINDA software. Finally, for 8 subjects with an intact gallbladder, dosimetry estimates were also generated after the application of 2 different gallbladder models, a gallbladder-voiding model (50% of gallbladder activity was transferred into intestines every 3 h) and a simulated cholecystectomy (all gallbladder activity was transferred into intestines). A background (bkg) VOI consisting of at least 2,500 mL over the proximal thighs (including muscular, vascular, osseous, and adipose tissues) was drawn for the purpose of target-to-background ratio (TBR) calculation, defined as follows: TBR maximum (TBRmax) = maximum uterus SUV ($SUVmax_{uterus}$)/mean bkg SUV ($SUVmean_{bkg}$) and TBR mean (TBRmean) = mean uterus SUV ($SUVmean_{uterus}$)/$SUVmean_{bkg}$.

Biologic Samples

Tests negative for qualitative urine β-human chorionic gonadotrophin were obtained before the 4FMFES injection in all premenopausal subjects. In all subjects, serum estradiol was measured at baseline (before the 4FMFES injection). Blood count, serum biochemical analysis (sodium, potassium, chloride ions, glucose, creatinine, γ-glutamyl transpeptidase, aspartate transaminase, alanine transaminase, and alkaline phosphatase), and urinalysis were performed on samples obtained at baseline and approximately 2.5 and 24 h after the 4FMFES injection. Finally, 4 serial blood samples were also obtained after each PET acquisition to measure blood and plasma activity. All samples were withdrawn from the arm not used for the 4FMFES injection. Plasma was separated by centrifugation. Blood and plasma samples, along with a standard of known activity, were counted in a γ-well counter (Cobra; Packard). One-phase exponential decay nonlinear regression was performed on the pooled plasma and blood activity measurements taken at more than 30 min after the 4FMFES injection. Initial plasmatic activity concentration was extrapolated to calculate the apparent plasmatic volume of distribution.

Safety Monitoring

Vital signs (heart rate, blood pressure, and arterial oxygen saturation) were monitored at baseline and after each PET acquisition. Subjects were asked to report any discomfort or side effect from the moment of the injection, during all the imaging procedures, at the 24-h visit, and during a follow-up phone call 1 wk later.

Statistical Methods

Data are reported as mean ± SD unless otherwise specified. GraphPad Prism 5 software (GraphPad Software Inc.) was used to perform statistical analyses and graph data. One-tailed paired *t* tests were used to determine whether there was a significant decrease in liver and renal function test parameters. Two-tailed unpaired *t* tests were used to assess any significant differences in uterus uptake between pre- and postmenopausal subjects. Spearman tests (nonparametric correlations) were performed to assess whether uterus uptake was influenced by serum estradiol level, injected estradiol-equivalent mass, or serum estradiol level corrected for

injected estradiol-equivalent mass (calculated with 4FMFES plasmatic apparent volume of distribution). A P value less than or equal to 0.05 was considered statistically significant.

RESULTS

Biodistribution

Figure 1 shows the typical biodistribution of 4FMFES over time, as assessed with 4 sequential rapid PET acquisitions over 2 h. Variable amounts of activity are deposited along the veins of the injected arm, proximal to the site of injection, as seen with other ER imaging agents (*11*). The liver showed a rapid and intense uptake, which decreased slowly over time as the massive biliary elimination occurred. This uptake resulted in intense activity accumulation in both the gallbladder (with the exception of 2 subjects who had undergone prior cholecystectomy) and intestines. Although low urinary excretion occurred (3.2 ± 2.2 %ID was collected in urine before the fourth PET acquisition), activity in the renal parenchyma remained at background levels. Figure 2 depicts the 4FMFES dose distribution over time. The biodistribution at 60 min after injection is summarized in Table 1.

Figure 3 shows the 4FMFES uptake in the uterus at 60 min after injection in another subject. The uterus was visualized in both premenopausal and postmenopausal subjects and generally exhibited a moderate uptake, which remained relatively stable over time. Because the background activity level tended to decrease over time, this resulted in a continually increasing TBR. There were no significant differences in $\%ID_{uterus}$, $SUVmean_{uterus}$, $SUVmax_{uterus}$, TBRmean, and TBRmax at any time point between pre- and postmenopausal subjects ($P > 0.05$, 2-tailed unpaired t tests), with 1 exception. We found a significant difference between the $\%ID_{uterus}$ at 120 min after injection between pre- and postmenopausal subjects (0.075 ± 0.033 %ID and 0.163 ± 0.026 %ID, respectively; $P = 0.003$, 2-tailed unpaired t test). The 4FMFES uterus uptake is detailed in Figure 4 and Table 2.

4FMFES showed a rapid blood clearance, as vascular activity was barely visible on the first PET acquisition and then indistinguishable from the low-level background activity on the subsequent PET acquisitions (Fig. 1; Table 2). These observations are consistent with the results from the serial blood and plasma activity measurements. Between 30 and 150 min after the 4FMFES injection, the measurements of blood and plasma activity concentration could be reasonably well fitted in a 1-phase exponential-decay model. At 60 min after injection, the blood and plasma activities were extrapolated at 5.6×10^{-4} (95% confidence interval [CI], 5.0–6.2 × 10^{-4}) and 7.3×10^{-4} (95% CI, 6.5–8.1 × 10^{-4}) %ID/g, respectively, and were decaying with a half-life of 112 (95% CI, 76–215) and 108 (95% CI, 72–216) min, respectively. From the plasma clearance curve, the initial plasma activity concentration was extrapolated to 1.07×10^{-3} %ID/g. Therefore, we could estimate the apparent plasmatic volume of distribution of 4FMFES at 1.60 L/kg.

No significant correlations were found between uterus uptake variables ($\%ID_{uterus}$, $SUVmean_{uterus}$, $SUVmax_{uterus}$, TBRmean, and TBRmax) at any time point and baseline serum estradiol level, estradiol-equivalent injected mass, or serum estradiol level corrected for injected estradiol-equivalent mass ($P > 0.05$, Spearman tests).

Dosimetry

The absorbed radiation dose estimates for 4FMFES are presented in Table 3 (including all subjects, $n = 10$). The gallbladder was, by far, the critical organ, followed by the upper large intestine, small intestine, and liver.

Table 4 illustrates the influence of gallbladder activity accumulation on the dosimetry estimates. In the 8 fasting subjects who had not undergone cholecystectomies, the radiation-absorbed dose to the gallbladder was high (0.99 ± 0.24 mSv/MBq). In the absence of the gallbladder, the upper large intestine became the critical organ. Interestingly, when we simulated a cholecystectomy in these subjects, by transferring all the gallbladder activity directly to the intestines, the dose to small, upper large, and lower large intestines rose to reach the levels of the 2 subjects who had undergone cholecystectomies. Not surprisingly, when we applied a gallbladder-voiding model to simulate regular meal intake after the procedure in subjects who had not undergone cholecystectomies, this resulted in intermediate values: a reduction in the absorbed dose to the gallbladder but an

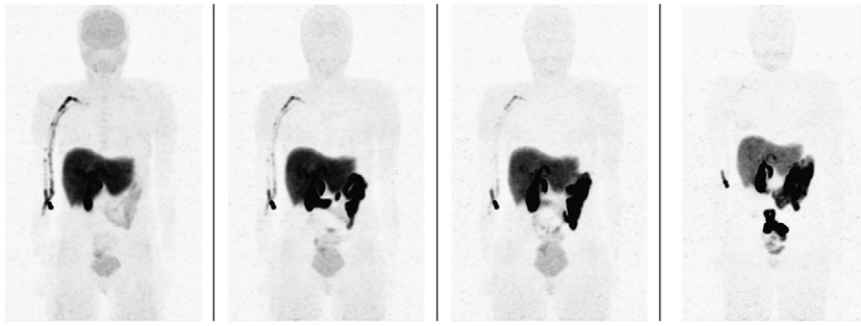

FIGURE 1. Anterior maximum-intensity projections of PET at 6, 27, 57, and 118 min after injection (from left to right), in premenopausal subject. Intensity scale was adjusted at same level for all images. Liver uptake was rapid and intense, and this was followed by massive biliary excretion. There was little urinary excretion. Transient and mild hyperactivity was seen in some highly perfused organs, such as brain, but vascular activity vanished quickly, resulting in rather uniform and low-level background activity from 30 min and thereafter. Uterine uptake was seen in projection of right upper portion of urinary bladder. Activity was deposited along proximal veins of injected arm, as seen with other ER imaging agents.

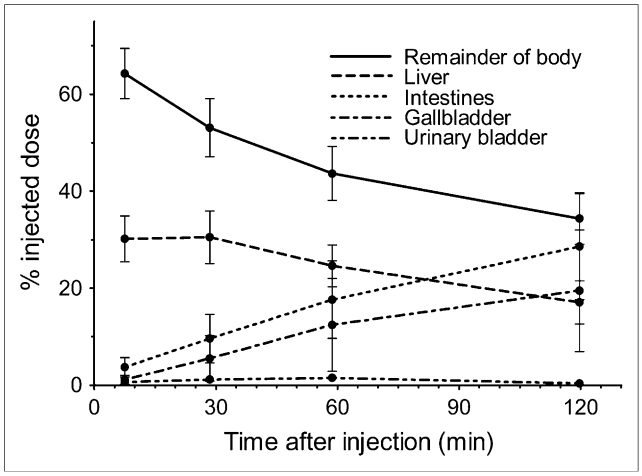

FIGURE 2. %ID in source organs and in remainder of body as function of time after 4FMFES injection. Liver and remainder of body activity decreased over time, as hepatobiliary excretion occurred, resulting in continuously increasing accumulation in both gallbladder and intestines. Urinary excretion was low. Data for uterus are presented in Figure 4.

increase in the doses to the small intestine and upper larger intestine. Other organs were also influenced by the redistribution of activity between the gallbladder and intestines, as shown in Table 4. However, this had little repercussion on the ED.

Safety

4FMFES was well tolerated in all subjects, although most subjects reported a light discomfort in the arm during injection, which resolved rapidly after the end of the injection. This discomfort was due to the small amount of ethanol in the 4FMFES solution. One subject reported redness and itching on the skin surrounding the injection site within hours after injection, most likely due to a reaction to the tape holding the catheter in place rather than the radiopharmaceutical itself. No significant increase in serum aspartate transaminase, alanine transaminase, γ-glutamyl transpeptidase, alkaline phosphatase, and creatinine levels at 2.5 and 24 h after 4FMFES injection was observed ($P > 0.05$, 1-tailed paired t test). Although there was a mild but significant increase in total serum bilirubin level at 2.5 h after injection (30% increase, from 5.2 ± 4.0 to 6.7 ± 3.6 μmol/L; $P = 0.02$, 1-tailed paired t test), it was not considered of any clinical importance, because it resolved at 24 h after injection (5.1 ± 2.9 μmol/L). Also, in all subjects and at all times the serum bilirubin levels stayed well below the upper normal limit of 17 μmol/L. Serum glucose, sodium, potassium, and chloride levels and blood counts all varied within 7% or less of their baseline values at 2.5 and 24 h—a degree of variation that was considered within physiologic limits. Results of urinalysis were unremarkable at the 3 time points (baseline, 2.5 h after injection, and 24 h after injection) in all subjects. Vital-sign variations from baseline to approximately 20, 45, 75, and 135 min after injection were unremarkable (>1% variation in arterial oxygen saturation; >7% in heart rate and blood pressure).

DISCUSSION

The majority of breast cancers express ERs or progesterone receptors. Hormone receptor status is the most important predictive factor of response to hormone therapy and also has a strong prognostic significance in patients with breast cancer (*12*). Although hormone receptor status of primary breast tumors is routinely assessed by immunohistochemistry, it is not always possible to assess the hormone receptor content of metastatic lesions noninvasively. Because breast cancer is often a heterogeneous disease (*13*), noninvasive whole-body molecular imaging techniques such as ER scintigraphy have the potential to affect the management of patients with breast cancer.

To date, FES has been the most successful ER imaging agent for PET (*2,14*). FES uptake has been shown to cor-

TABLE 1. 4FMFES Biodistribution at 60 Minutes After Injection (±SD)

Region of biodistribution	%ID	%ID/g	SUVmean	SUVmax
Source organs				
Gallbladder content	12.5 ± 9.6	1.96E−01 ± 1.19E−01	109 ± 59	476 ± 269
Liver	24.6 ± 4.3	1.73E−02 ± 3.67E−03	9.92 ± 1.62	172 ± 123
Uterus	0.12 ± 0.05	4.61E−03 ± 1.08E−03	2.68 ± 0.68	5.34 ± 1.24
Urinary bladder content	1.50 ± 0.46	8.83E−03 ± 9.83E−03	4.89 ± 4.88	14.2 ± 20.4
Intestinal content*	17.6 ± 8.0	2.20E−02 ± 6.07E−03	12.9 ± 4.2	197 ± 250
Nonsource regions				
Background†	—	7.68E−04 ± 1.35E−04	0.45 ± 0.10	1.63 ± 0.55
Remainder of body‡	43.7 ± 5.5	7.90E−04 ± 9.72E−05	0.46 ± 0.06	—

*Intestinal VOI was encompassing small- and large-intestine activity.
†Background VOI was a volume of at least 2,500 mL over proximal thighs, comprising vascular, muscular, bony, and fatty tissues.
‡Remainder of body %ID = 100% – source organ ID%; remainder of body volume = body weight (g) – source organ volumes.
Times are mean ± SD.

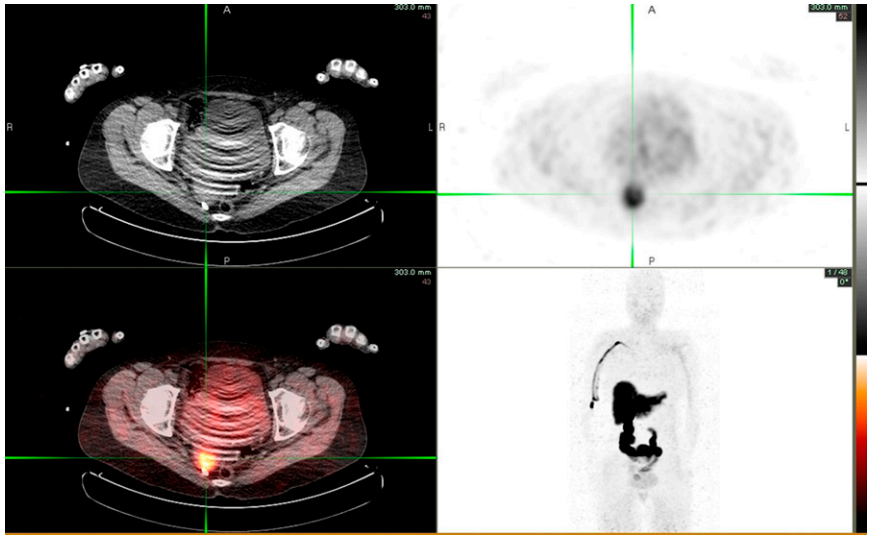

FIGURE 3. 4FMFES uterine uptake (green cross lines) in postmenopausal subject, on PET/CT transaxial slice at 60 min after injection. Tracer uptake was more prominent in endometrium (SUVmax = 6.2). Urinary activity was relatively low.

relate with in vitro ER concentration assessment (*2,15*). FES PET provides complementary information to metabolic activity assessment with ^{18}F-FDG PET (*16,17*).

Other radiolabeled estrogens may have favorable imaging properties to improve on FES, which has high levels of circulating metabolites in the blood (*18*). We developed a new ER imaging tracer for PET, 4FMFES, with improved TBRs in animal experiments (*3–5*). Before studying 4FMFES PET in patients with breast cancer, we decided to conduct a phase I study in healthy volunteer women, primarily to assess the radiation dosimetry and safety of 4FMFES but also to obtain physiologic biodistribution data in controlled conditions to get more insight about various factors that could affect the capacity of 4FMFES to image ER-positive tumors in humans.

The most interesting feature of 4FMFES as an ER imaging agent is its significant uptake by the uterus, the physiologic target in healthy women. The uterus was the only organ that showed significant and rapid 4FMFES uptake and retention over time, in contrast to the liver and background, which showed decreasing activity. The uterus was visualized in both premenopausal and postmenopausal subjects. These observations suggest an ER-mediated specific uptake. Mankoff et al. (*6*) found an FES uterine uptake of up to 3.2×10^{-4} %ID/g at 60 min after injection (data extracted from a graph, 0.12 kBq/g per 37 MBq). Even if the comparison has limitations because the respective measurements were made in different settings, 4FMFES uterine uptake appeared higher, at $4.6 \pm 3.0 \times 10^{-3}$ %ID/g. Comparison of our observed 4FMFES blood-level activity concentrations ($\sim 6 \times 10^{-4}$ %ID/g between 60 and 120 min after 4FMFES injection) with data presented by Mankoff et al. (*6*) on FES extracted from a blood time–activity curve ($\sim 18 \times 10^{-4}$ %ID/g at 60–120 min after FES injection) shows good agreement with our previous observations in mice, where blood-activity levels of 4FMFES were about half of FES levels (*4,5*).

TABLE 2. 4FMFES Uterine Uptake as Function of Time After Injection

	Time (min)			
Region	7.5	30	60	120
Uterus				
%ID	0.114 ± 0.064	0.114 ± 0.058	0.122 ± 0.047	0.110 ± 0.018
%ID/g	4.47E−03 ± 3.13E−03	4.60E−03 ± 3.14E−03	4.61E−03 ± 2.97E−03	4.70E−03 ± 2.51E−03
SUVmean	2.60 ± 1.88	2.67 ± 1.89	2.68 ± 1.65	2.75 ± 1.47
SUVmax	5.38 ± 3.01	5.24 ± 3.14	5.34 ± 3.32	6.03 ± 3.02
Background				
%ID/g	1.21E−03 ± 2.26E−04	9.62E−04 ± 1.57E−04	7.68E−04 ± 1.35E−04	4.91E−04 ± 9.82E−05
SUVmean	0.71 ± 0.16	0.56 ± 0.12	0.45 ± 0.10	0.29 ± 0.08
TBRmax	7.62 ± 4.21	9.42 ± 2.73	12.10 ± 2.23	21.78 ± 5.96
TBRmean	3.79 ± 0.99	4.87 ± 1.04	6.12 ± 1.49	9.71 ± 2.43

Times are mean ± SD.

TABLE 3. Radiation Dosimetry Estimates

Organ	4FMFES	FES (6)
Absorbed dose (mGy/MBq ± SD)		
Adrenals	0.019 ± 0.002	0.023 ± 0.003
Brain	0.005 ± 0.001	0.010 ± 0.001
Breasts	0.007 ± 0.000	0.009 ± 0.002
Gallbladder wall	0.797 ± 0.505	0.102 ± 0.041
Lower large intestine	0.043 ± 0.014	0.012 ± 0.001
Small intestine	0.118 ± 0.039	0.027 ± 0.015
Stomach wall	0.019 ± 0.001	0.014 ± 0.001
Upper large intestine	0.131 ± 0.040	0.030 ± 0.016
Heart wall	0.013 ± 0.001	0.026 ± 0.004
Kidneys	0.020 ± 0.001	0.035 ± 0.004
Liver	0.095 ± 0.019	0.126 ± 0.030
Lungs	0.011 ± 0.001	0.017 ± 0.002
Muscle	0.011 ± 0.000	0.021 ± 0.001
Ovaries	0.028 ± 0.006	0.018 ± 0.002
Pancreas	0.024 ± 0.005	0.023 ± 0.002
Red marrow	0.012 ± 0.001	0.013 ± 0.002
Osteogenic cells	0.013 ± 0.001	0.014 ± 0.001
Skin	0.007 ± 0.001	0.005 ± 0.000
Spleen	0.012 ± 0.000	0.015 ± 0.003
Thymus	0.008 ± 0.001	0.014 ± 0.001
Thyroid	0.006 ± 0.001	0.012 ± 0.001
Urinary bladder wall	0.028 ± 0.006	0.050 ± 0.020
Uterus	0.026 ± 0.006	0.039 ± 0.013
Effective dose (mSv/MBq ± SD)	0.026 ± 0.004	0.022 ± 0.004

Because of the low sex hormone–binding globulin (SHBG) affinity of 4FMFES (*1,4*), there is some uncertainty regarding the applicability of results in small-animal studies to humans. Nevertheless, our preliminary results do not support the hypothesis that SHBG affinity is an essential property for a successful ER imaging agent, as hypothesized by others (*11*).

Dosimetry

The dose to the gallbladder was found to be higher than doses previously reported with other ER imaging agents, including FES (*6,19,20*), and appeared mainly because of the more extensive hepatobiliary excretion of activity with 4FMFES. The fact that participants fasted before the 4FMFES injection, probably contributed to maximizing the activity accumulation in the gallbladder. The dose to the gallbladder after the 4FMFES injection was even higher than the highest dose reported with a ^{99m}Tc hepatobiliary agent (diisopropyliminodiacetic acid, 0.56 mGy/MBq) (*21*). Compared with FES, we also found higher doses to the intestines, stomach, ovaries, and pancreas with 4FMFES but lower doses to most other organs, as was consistent with the faster plasma clearance of 4FMFES.

To determine the effect on dosimetry of repeated food ingestion after a 4FMFES injection performed under fasting conditions, we applied a gallbladder ejection fraction within the reference range (arbitrarily set to 50%) at 3-h intervals after injection. Because the majority of the absorbed dose was received before the first simulated meal, the impact on gallbladder dose was only moderate (Table 4), but the overall dosimetry values approached the values presented in Table 3, which included our whole study population (20% without gallbladder; 80% with gallbladder). We also explored another gallbladder model, in which we simulated a cholecystectomy in our 8 subjects with an intact gallbladder (Table 4). Interestingly, the dosimetry estimates approached those of the 2 subjects who had undergone cholecystectomies. In our 8 fasting subjects who had not undergone cholecystectomies, we observed that gallbladder and intestines each accumulated 50% of activity excreted by the liver, similar to what was reported by others (*21*). This percentage is greater than that reported by Wu et al., who found an average accumulation of 35% of activity in the gallbladder of fasting patients (*22*). Redis-

TABLE 4. Comparison of 4FMFES Radiation Dosimetry Estimates Between Subjects with Intact Gallbladder, Using Various Gallbladder Models, and Subjects with Prior Cholecystectomy

	Subjects with intact gallbladder (n = 8)			
Organ	No gallbladder model	Gallbladder-voiding model*	Simulated cholecystectomy†	Subjects with prior cholecystectomy (n = 2)
Absorbed dose (mGy/MBq ± SD)‡				
Adrenals	0.020 ± 0.002	0.019 ± 0.001	0.016 ± 0.001	0.016 ± 0.001
Gallbladder wall	0.988 ± 0.348	0.709 ± 0.247	—	—
Lower large intestine	0.038 ± 0.010	0.046 ± 0.007	0.066 ± 0.004	0.063 ± 0.009
Small intestine	0.104 ± 0.027	0.127 ± 0.020	0.184 ± 0.014	0.173 ± 0.028
Upper large intestine	0.117 ± 0.028	0.141 ± 0.020	0.200 ± 0.015	0.187 ± 0.031
Ovaries	0.025 ± 0.004	0.029 ± 0.003	0.038 ± 0.002	0.037 ± 0.004
Pancreas	0.026 ± 0.003	0.024 ± 0.002	0.018 ± 0.000	0.017 ± 0.001
Uterus	0.024 ± 0.004	0.027 ± 0.003	0.033 ± 0.004	0.034 ± 0.006
Effective dose (mSv/MBq ± SD)	0.025 ± 0.003	0.027 ± 0.002	0.033 ± 0.001	0.031 ± 0.002

*Gallbladder-voiding model: 50% of gallbladder activity was transferred to intestines every 3 h.
†Simulated cholecystectomy: total gallbladder activity was transferred to intestines.
‡For all other organs, absorbed dose varied by less than 12% when either gallbladder model was applied.

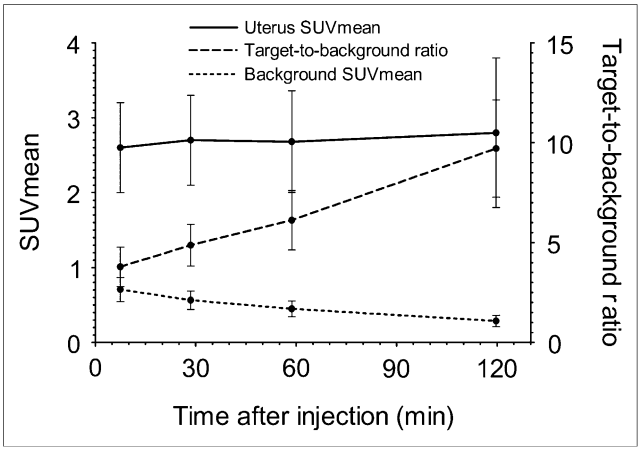

FIGURE 4. $SUVmean_{uterus}$, $SUVmean_{bkg}$, and TBRmean = $SUVmean_{uterus}/SUVmean_{bkg}$ as function of time after 4FMFES injection. Uterine uptake remained relatively constant over time, whereas background level tended to decrease, resulting in increasing TBR.

tributing the activity excreted by the liver between the gallbladder and intestines according to the latter proportion would have also had significantly lowered the estimated absorbed dose to the gallbladder.

Although limiting the injected dose of 4FMFES to reduce the radiation dose to the gallbladder might not be ideal for maintaining good image quality, we would certainly recommend performing 4FMFES PET/CT under nonfasting conditions. The patients were required to fast only to ensure controlled study conditions, but fasting is generally not required for ER imaging.

We administered 4 MBq of 4FMFES per kilogram, with a maximum of 185 MBq. For this maximal dose, the ED would be 4.8 ± 0.7 mSv, which remains within acceptable limits for clinical use and within the range of other diagnostic imaging procedures, including FES PET with similar injected doses. The ED did not vary much between different subgroups and gallbladder models (Table 4). This is because the gallbladder is not accounted for in the ED calculation. This is not the case with the effective dose equivalent model (EDE; also calculated by OLINDA software), in which a 6% dose to the gallbladder accounted for 50%−75% of the EDE in the participants who had not undergone cholecystectomies, yielding an overall EDE of 15.2 ± 4.4 mSv per 185 MBq.

There are few reports of studies using serial whole-body PET/CT acquisitions to assess biodistribution and dosimetry in human subjects (*23,24*). This study demonstrates the convenience of determining the whole-body biodistribution and the dosimetry estimates of novel PET tracers by successive rapid whole-body PET/CT acquisitions. Despite the lower image quality of the extremely low–dose CT images in this study, we found their fusion with PET images useful in achieving a more precise delineation of source organs. The image fusion allowed us to identify the uterus with confidence, particularly on the last PET acquisition, on which the intestinal activity in the pelvis was more prominent. A whole-body acquisition begun shortly after the tracer administration resulted in reliable and reproducible time–activity curves and residence-time calculations.

Safety

The reported discomfort related to the small ethanol content (<1 mL) of the 4FMFES preparation was not unexpected and was well accepted by all the subjects. No pharmacologic effects were expected because of the low amounts of estrogen receptor-binding mass coinjected with the radiolabeled 4FMFES. We previously conducted an animal toxicity study, in which we injected mice with cold 4FMFES doses equivalent to more than 1,000 times the actual human radiolabeled 4FMFES doses without observing any toxic effects (F. Bénard and J. Rousseau, unpublished data, 2004). The slight and transient observed bilirubin elevation was of no clinical significance. It would be prudent, however, to continue monitoring serum bilirubin in future studies, to further clarify this finding. In light of animal data and our preliminary clinical experience in human subjects, we consider 4FMFES safe for human use.

CONCLUSION

This study evaluated the biodistribution of 4FMFES in healthy women. 4FMFES exhibited significant, most likely ER-mediated, uterus uptake in both pre- and postmenopausal subjects in our study. This finding is in agreement with small-animal experiments and further highlights the potential of 4FMFES for ER imaging in patients with breast cancer. No major adverse reactions were observed with 4FMFES in this study. A 4FMFES dose of up to 185 MBq results in an acceptable ED and should allow good image quality using standard whole-body PET acquisition protocols. A 4FMFES injection administered to a nonfasting subject is recommended, as it may help to decrease the absorbed dose to the gallbladder, the critical organ. A clinical study directly comparing 4FMFES and FES in patients with breast cancer, to establish which radiopharmaceutical is optimal in determining ER content in breast cancer metastases, is projected.

ACKNOWLEDGMENTS

We thank Réjean Langlois for helping with the 4FMFES radiolabeling and Chantale Langevin for her assistance in conducting each PET study. This project was supported by the Canadian Breast Cancer Research Alliance (CBCRA) grant 015388 and a Fonds de la recherche en santé du Québec scholarship.

REFERENCES

1. Beauregard J-M, Turcotte É, Bénard F. Steroid receptor imaging in breast cancer. *PET Clinics.* 2006;1:51–70.

2. Mintun MA, Welch MJ, Siegel BA, et al. Breast cancer: PET imaging of estrogen receptors. *Radiology.* 1988;169:45–48.
3. Seimbille Y, Ali H, van Lier JE. Synthesis of 2,16α- and 4,16α-difluoroestradiols and their 11β-methoxy derivatives as potential estrogen receptor-binding radiopharmaceuticals. *J Chem Soc Perk Trans 1.* 2002:657–663.
4. Seimbille Y, Rousseau J, Bénard F, et al. ^{18}F-labeled difluoroestradiols: preparation and preclinical evaluation as estrogen receptor-binding radiopharmaceuticals. *Steroids.* 2002;67:765–775.
5. Benard F, Ahmed N, Beauregard JM, et al. [^{18}F]Fluorinated estradiol derivatives for oestrogen receptor imaging: impact of substituents, formulation and specific activity on the biodistribution in breast tumour-bearing mice. *Eur J Nucl Med Mol Imaging.* 2008;35:1473–1479.
6. Mankoff DA, Peterson LM, Tewson TJ, et al. [^{18}F]Fluoroestradiol radiation dosimetry in human PET studies. *J Nucl Med.* 2001;42:679–684.
7. Beauregard J-M, Croteau E, Ahmed N, van Lier J, Benard F. Biodistribution and dosimetry of 4-fluoro-11β-methoxy-16α-[^{18}F]fluoroestradiol (4FMFES) in healthy women [abstract]. *J Nucl Med.* 2008;49(suppl):15P.
8. Ahmed N, Langlois R, Rodrigue S, Benard F, van Lier JE. Automated synthesis of 11β-methoxy-4,16α-[16α-^{18}F]difluoroestradiol (4F-M[^{18}F]FES) for estrogen receptor imaging by positron emission tomography. *Nucl Med Biol.* 2007;34: 459–464.
9. Beauregard JM, Croteau E, Ahmed N, Ouellette R, van Lier JE, Benard F. Effective specific activities determined by scintillation proximity counting for production runs of [^{18}F]FES and 4F-M[^{18}F]FES. *Nucl Med Biol.* 2007;34: 325–329.
10. Stabin MG, Siegel JA. Physical models and dose factors for use in internal dose assessment. *Health Phys.* 2003;85:294–310.
11. Jonson SD, Bonasera TA, Dehdashti F, Cristel ME, Katzenellenbogen JA, Welch MJ. Comparative breast tumor imaging and comparative in vitro metabolism of 16α-[^{18}F]fluoroestradiol-17β and 16β-[^{18}F]fluoromoxestrol in isolated hepatocytes. *Nucl Med Biol.* 1999;26:123–130.
12. Wood WC, Muss HB, Solin LJ, Olopade OI. Malignant tumours of the breast. In: DeVita VT, Hellman S, Rosenberg SA, eds. *Cancer: Principles & Practice of Oncology.* 7th ed. Philadelphia, PA: Lippincott Williams & Wilkins; 2005:1415–1477.
13. Fisher B, Redmond CK, Fisher ER. Evolution of knowledge related to breast cancer heterogeneity: a 25-year retrospective. *J Clin Oncol.* 2008;26:2068–2071.
14. McGuire AH, Dehdashti F, Siegel BA, et al. Positron tomographic assessment of 16 α-[^{18}F] fluoro-17 β-estradiol uptake in metastatic breast carcinoma. *J Nucl Med.* 1991;32:1526–1531.
15. Peterson LM, Mankoff DA, Lawton T, et al. Quantitative imaging of estrogen receptor expression in breast cancer with PET and ^{18}F-fluoroestradiol. *J Nucl Med.* 2008;49:367–374.
16. Mortimer JE, Dehdashti F, Siegel BA, Katzenellenbogen JA, Fracasso P, Welch MJ. Positron emission tomography with 2-[^{18}F]fluoro-2-deoxy-D-glucose and 16α-[^{18}F]fluoro-17β-estradiol in breast cancer: correlation with estrogen receptor status and response to systemic therapy. *Clin Cancer Res.* 1996;2:933–939.
17. Linden HM, Stekhova SA, Link JM, et al. Quantitative fluoroestradiol positron emission tomography imaging predicts response to endocrine treatment in breast cancer. *J Clin Oncol.* 2006;24:2793–2799.
18. Mankoff DA, Tewson TJ, Eary JF. Analysis of blood clearance and labeled metabolites for the estrogen receptor tracer [F-18]-16 α-fluoroestradiol (FES). *Nucl Med Biol.* 1997;24:341–348.
19. Van de Wiele C, De Vos F, De Sutter J, et al. Biodistribution and dosimetry of (iodine-123)-iodomethyl-*N, N*-diethyltamoxifen, an (anti)oestrogen receptor radioligand. *Eur J Nucl Med.* 1999;26:1259–1264.
20. Rijks LJ, Busemann Sokole E, Stabin MG, de Bruin K, Janssen AG, van Royen EA. Biodistribution and dosimetry of iodine-123-labelled Z-MIVE: an oestrogen receptor radioligand for breast cancer imaging. *Eur J Nucl Med.* 1998;25:40–47.
21. Brown PH, Krishnamurthy GT, Bobba VR, Kingston E, Turner FE. Radiation-dose calculation for five Tc-99m IDA hepatobiliary agents. *J Nucl Med.* 1982; 23:1025–1030.
22. Wu RK, Siegel JA, Rattner Z, Malmud LS. Tc-99m HIDA dosimetry in patients with various hepatic disorders. *J Nucl Med.* 1984;25:905–912.
23. Nye JA, Schuster DM, Yu W, Camp VM, Goodman MM, Votaw JR. Biodistribution and radiation dosimetry of the synthetic nonmetabolized amino acid analogue anti-^{18}F-FACBC in humans. *J Nucl Med.* 2007;48:1017–1020.
24. Van Laere K, Koole M, Sanabria Bohorquez SM, et al. Whole-body biodistribution and radiation dosimetry of the human cannabinoid type-1 receptor ligand ^{18}F-MK-9470 in healthy subjects. *J Nucl Med.* 2008;49:439–445.